# 2D Partial Unwinding - A Novel Non-linear Phase Decomposition of Images

Yanting Li, Liming Zhang, Member, IEEE, and Tao Qian

*Abstract*—This paper aims at proposing a novel 2D non-linear phase decomposition of images, which performs the image processing tasks better than the traditional Fourier transformation (linear phase decomposition), but further, it has additional mathematical properties allowing more effective image analysis, including adaptive decomposition components and positive instantaneous phase derivatives. 1D unwinding Blaschke decomposition has recently been proposed and studied. Through factorization it expresses arbitrary 1D signal into an infinite linear combination of Blaschke products. It offers fast converging positive frequency decomposition in the form of rational approximation. However, in the multi-dimensional cases the usual factorization mechanism does not work. As a consequence, there is no genuine unwinding decomposition for multi-dimensions. In this study a 2D partial unwinding decomposition based on algebraic transforms reducing multi-dimensions to the 1D case is proposed and analyzed. The result shows that the fast convergence offers efficient image reconstruction. The tensor type decomposing terms are mutually orthogonal, giving rise to 2D positive frequency decomposition. The comparison results show that the proposed method outperforms the standard greedy algorithm and the most commonly used methods in the Fourier category. An application in watermarking is presented to demonstrate its potential in applications.

*Index Terms*—Fourier transform, Hardy space, greedy algorithm, adaptive Fourier decomposition, unwinding Blaschke decomposition, Nevanlinna factorization.

## I. INTRODUCTION

**T**HE theories and methods of the one-dimensional (1D) and multi-dimensional ($m$D) Fourier transformation (FT) stand as traditional and powerful tools in both pure and applied mathematics. They are used for image processing with a wide range of particular tasks, including image analysis [1]–[4], filtering [5], [6], reconstruction [7], [8], and compression [9], etc. Due to the fact that trigonometrical functions are eigen-functions of the Dirac (the simplest first order differential) operators, and due to its wide and deep connections with all branches of mathematics, Fourier theory has been and will continue to have a fundamental role with great significance and deep involvement in both mathematics and its applications.

Non-linear phenomenon [10], [11] has been a great impetus for the development of sparse representations of signals. This

Y. Li is with the Department of Mathematics, Faculty of Science and Technology, University of Macau, Taipa, Macau, China (e-mail: ytli1227@126.com).
L. Zhang is with the Department of Computer and Information Science, Faculty of Science and Technology, University of Macau, Taipa, Macau, China (e-mail: lmzhang@umac.mo).
T. Qian is with the Macau Institute of Systems Engineering, Macau University of Science and Technology, Avenida Wai Long, Taipa, Macau, China (e-mail: tqian1958@gmail.com).

trend, together with the interests on non-linear phase and positive instantaneous frequency (IF) of signals, has motivated a type of signal representations phrased as adaptive Fourier decomposition (AFD). In this terminology the word "Fourier" refers to its connections with square-integrable analytic signals and positive IFs, indeed, FT is a special case of AFD when particular parameters are chosen; while the word "adaptive" refers to sparse and fast representation, which is, in particular, regardless whether the expanding basic functions constitute a basis. There are two main types of 1D-AFD of which one is the maximal selection type (MST) AFD (see, for instance, [12], [13]); and the other is the unwinding type AFD (called unwinding Blaschke decomposition (UBD) first by Coifman et al., see [14]–[16]). The maximal selection type 1D-AFD in each context is based on a Riemann-Lebesgue type lemma affiliated to the context; while unwinding Blaschke expansion, based on the factorization operation, consecutively extracts carrier frequencies and hence achieves a fast converging and positive frequency decomposition. In [17] the author proposes an algorithm that combines the two separated processes, i.e., maximal selection and factorization, together. In summary, [12]–[17] are 1D algorithms for 1D signal processing. On the other hand, this paper is 2D algorithm for image processing. This paper is the second such type 2D non-linear phase decomposition in the literature. The first one is [18], in which the approach is not based on unwinding but on some maximal selection principle. To our knowledge the present paper is the first 2D non-linear phase unwinding approach in the literature.

In the 1D cases, both the processes on maximal selection and factorization are fully developed and analyzed with demonstrative applications [12]–[17], [19]–[23]. In higher dimensions, one can proceed maximal selection type AFD that mainly results in fast converging rational approximations. Then he can further extend such sparse representation method to general reproducing kernel Hilbert spaces. The corresponding algorithms, either with the several complex variables setting or the Clifford algebra setting have yet to be developed. On the other hand, there does not exist a genuine $m$D unwinding AFD being analogous to the 1D cases. This defeat is due to the following reason. In one complex variable, if $f$ is analytic at $a$ and $f(a) = 0$, then there exists a function $g$, being analytic at $a$, and $f(z) = (z - a)g(z)$. In higher dimensions, no matter with the several complex variables setting or the Clifford algebra setting, there does not exist analogous factorization result. There exist matrix-valued Blaschke products [24], [25], however, the unwinding process cannot proceed without an analogous factorization result.

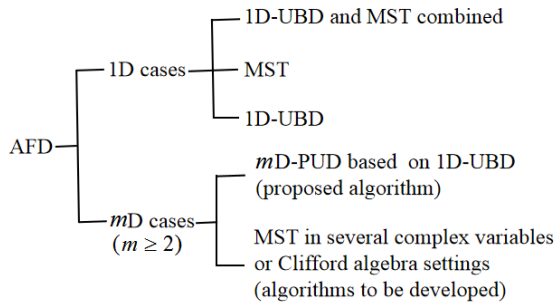The purpose of the present study is to develop what we

Fig. 1.  The relationships among different AFDs in $m$D cases ($m \geq 1$).

call "2D partial unwinding decomposition", abbreviated as 2D-PUD, that adopts the 1D unwinding Blaschke decomposition (1D-UBD), through elementary algebraic operations, to the 2D case. It turns out that the type of expansion has fast convergence with excellent image reconstruction effect. Besides, 2D-PUD gives rise to non-linear phase decompositions with positive partial instantaneous frequency, which has never been studied in the literature and is expected to lead to a new research area in the image processing. The related theory and applications of this aspect will be developed in our forthcoming work. The relationships among the above mentioned AFD algorithms are illustrated in Fig. 1.

In this paper, the convergence of the proposed 2D-PUD and orthogonality of the decomposing components are proved. The computational complexity is provided. To demonstrate the effectiveness and efficiency of the proposed algorithm, two sets of the experiments are conducted. The first one compares the efficiency of the image decomposition and reconstruction among 2D Fourier series (2D-FS), 2D greedy algorithm (2D-GA) (or match pursuit) [26]–[31] on the product-Szegö dictionary, slice-1D-AFD, slice-1D-UBD, and our proposed 2D-PUD. The results show that 2D-PUD has the best reconstruction effect. The second experiment demonstrates the effectiveness of our proposed algorithm on an application in watermarking by comparing it with the popular discrete cosine transform (DCT) based watermarking technique. The results show that the embedded watermarks can be better protected by our proposed approach. Besides, the embedded image size can be as large as the original image. The experiments exhibit great potential of the proposed approach in the future.

The rest of the paper is organized as follows. In Section II, the mathematical foundation of 2D-PUD with the Hardy $H^2$ space setting is introduced. In Section III, the proposed 2D-PUD in the $L^2$ setting is presented in detail. Experimental results are shown in Section IV. Conclusions and prospects of the future work are drawn in Section V.

## II. PRELIMINARIES

As the proposed 2D-PUD is through the 1D-UBD, we will briefly introduce the fundamental knowledge of 1D-UBD. Since the unwinding decompositions are for complex analytic functions belonging to appropriate complex Hardy spaces $H^2$, while the real world signals are assumed to be of finite energy, or belong to the Lebesgue $L^2$ spaces, this section also clarifies

the relationship between the Hardy spaces and the Lebesgue $L^2$ spaces.

### A. From 1D Fourier series to 1D Unwinding Blaschke Decomposition

Denote by $\mathbb{D}$ the unit disc, $\mathbb{T}$ its boundary, i.e., the unit circle, and $\mathbb{C}$ the complex plane. Any complex-valued function of finite energy on the circle, $f(e^{it})$, in $L^2(\mathbb{T})$ is expressible as an energy converging series. The latter is further split into two pieces, being in the Hardy spaces of, respectively , the interior and the exterior unit disc, i.e., $f = f^+ + f^-$, as

$$
\begin{aligned}
f(e^{it}) &= \sum_{k=-\infty}^{\infty} c_k e^{ikt} = \sum_{k=0}^{\infty} c_k e^{ikt} + \sum_{k=-\infty}^{-1} c_k e^{ikt} \\
&= f^+(e^{it}) + f^-(e^{it}).
\end{aligned}
\tag{1}
$$

If $f$ is, practically, a real-valued function, due to the relation $c_{-k} = \overline{c}_k$, there holds

$$
f = 2\mathrm{Re}\, f^+ - c_0,
\tag{2}
$$

where Re means taking the real part of the complex-valued function $f^+$. The finite energy property is equivalent with the condition $\sum_{k=-\infty}^{\infty} |c_k|^2 < \infty$. The relation (2) shows that the study of $f$ is reduced to the study of $f^+$, the latter being called *the analytic signal associated with $f$*. It turns out that the analytic signals are identical with the non-tangential boundary limits of the analytic functions in the complex Hardy space of the interior unit disc. Among various definitions of the complex Hardy spaces in the interior unit disc we will use

$$
\begin{aligned}
H^2(\mathbb{D}) = \{f(z) \; : \; & f \text{ is analytic in } \mathbb{D}, \text{ and} \\
& f(z) = \sum_{k=0}^{\infty} c_k z^k, \sum_{k=0}^{\infty} |c_k|^2 < \infty\}.
\end{aligned}
\tag{3}
$$

There exists a natural isometric isomorphism between the above defined Hardy space in the disc and the so called *boundary Hardy space*, defined as

$$
H^2(\mathbb{T}) = \{f(e^{it}) \; : \; f(e^{it}) = \sum_{k=0}^{+\infty} c_k e^{ikt}, \; \sum_{k=0}^{\infty} |c_k|^2 < \infty\}.
\tag{4}
$$

We therefore consider the two function spaces as the same [32].

From the Nevanlinna factorization theorem [32], $f^+(z)$ can be decomposed into a product of an inner function $I(z)$ and an outer function $O(z)$. The outer function is given by

$$
O(z) = \exp\left\{\frac{1}{2\pi} \int_{-\pi}^{\pi} \frac{e^{it} + z}{e^{it} - z} \log |f^+(e^{it})| dt\right\}.
\tag{5}
$$

The inner function $I(z)$ can be further decomposed into $I(z) = B(z)S(z)$, where

$$
B(z) = z^m \prod_{z_k \neq 0} \frac{|z_k|}{z_k} \frac{z_k - z}{1 - \overline{z}_k z}
\tag{6}
$$

is the Blaschke product part, collecting all the zeros of $f^+(z)$; and $S(z)$ is the singular inner function part given by a regular Borel measure on the circle singular to the Lebesgue measure.

Notice that $O(z)$ and $S(z)$ are non-vanishing in the unit disc, and each of $B(z)$, $S(z)$, and $O(z)$ is unique up to a unimodular constant. Accordingly, we can write $f^+(z) = B(z)G(z)$, where $G(z) = S(z)O(z)$. The 1D-UBD is given by the iterative process

$$\begin{aligned} f^+ &= B_1 G_1 \\ &= B_1\big[G_1(0) + \big(G_1(z) - G_1(0)\big)\big] \\ &= B_1\big[G_1(0) + B_2 G_2\big] \\ &= a_1 B_1 + B_1 B_2\big[G_2(0) + \big(G_2(z) - G_2(0)\big)\big] \quad (7) \\ &\cdots \\ &= a_1 B_1 + a_2 B_1 B_2 + \cdots + B_1 B_2 \cdots B_N G_N, \end{aligned}$$

where $a_k = G_k(0)$, $k \geq 1$, and each $B_k$, $k \geq 2$, is the Blaschke product generated by the zeros of the function $G_k(z) - G_k(0)$ in $H^2(\mathbb{D})$. It was proved in [17] and [15] that $\lim_{N\to\infty} \|B_1 B_2 \cdots B_N G_N\| = 0$. Hence, in the $L^2$-norm sense,

$$f^+(z) = \sum_{k=1}^{\infty} a_k B_1 B_2 \cdots B_k. \quad (8)$$

If the analytic signal $f^+$ is analytically extendable to an open neighborhood of the closed unit disc, then the exponential decay rate is attained [17]. Note that if each $B_k$ only factorizes the factor $z$, which can be practically done, then the decomposition (7) reduces to 1D-FS. Thus the 1D-FS is a particular case of 1D-UBD. Due to the positive instantaneous frequency property of Blaschke products [33], 1D-UBD gives rise to fast converging positive instantaneous frequency decomposition of signals.

In practice, $f^+$ is usually supposed to have only a trivial singular inner function $S(z)$, namely $G(z) = O(z)$. In other words, the analytical signal $f^+$ can be factorized into the product of a Blaschke product and an outer function. In the algorithm design, a natural method is to first compute the outer function $G$ and then obtain the Blaschke product $B$ with the relation $B = f^+/G$. Indeed, computing the boundary limit function $G(e^{it})$ is reduced to computing the Hilbert transform of $\log|f^+(e^{it})|$. Practically, the non-tangential limit function $f^+(e^{it})$ may be close to zero, and as a consequence, the computation of $G(e^{it})$ become unstable. For this reason, a number of computative algorithms have been developed to compute Hilbert transforms. A method in [14] is to smooth $\log|f^+(e^{it})|$ by adding a small positive constant and another method in [34] is to add a small pure sinusoid to $\log|f^+(e^{it})|$. However, adding a small positive constant or a small pure sinusoid in each iteration may induce a big error after iterations. To avoid this defect Mai et al. [35] proposes to first factorize out a finite Blaschke product through finding a finite number of zeros of $f^+$ and then obtain $G(z)$ with the relation $G(z) = f^+(z)/B(z)$. [35] shows that the method of only unwinding a finite Blaschke product part can guarantee applicability of the algorithm.

In summary, the 1D-UBD (7) and its variations generate adaptive orthonormal systems by factorizing out all or part of the zero-factors in each decomposition iteration. Among various kinds of Fourier type positive-frequency expansions [12], [17], [19], [36], the 1D-UBD exhibits the fastest speed of convergence. Ever since the breaking through study of [14], the algorithm of 1D-UBD has been being optimized, and has been attracting a lot of interests and studies [35], [37].

### B. The Relationship between Spaces $H^2(\mathbb{D}^2)$ and $L^2(\mathbb{T}^2)$

As in the 1D case, practical 2D images are real-valued and defined in the 2D $L^2$ spaces. In this subsection, we provide a brief review of the relationship between the 2D $H^2$ and $L^2$ spaces. Based on the relationship, we reduce the analysis of $L^2$ to that of $H^2$. For the materials presented in this part, refer to [18].

Let $\mathbb{D}^2 := \mathbb{D} \times \mathbb{D} = \big\{(z,w) : |z| < 1, |w| < 1\big\}$ and $L^2(\mathbb{T}^2)$ denote the space of complex-valued functions on the 2-torus with finite energy, where the energy is defined via the inner product

$$\langle f, g \rangle = \frac{1}{4\pi^2} \int_{-\pi}^{\pi} \int_{-\pi}^{\pi} f(e^{it}, e^{is})\overline{g}(e^{it}, e^{is})dtds. \quad (9)$$

By the Plancherel theorem of the context, $f \in L^2(\mathbb{T}^2)$ if and only if in the $L^2$-norm sense,

$$f(e^{it}, e^{is}) = \sum_{-\infty < k,l < \infty} c_{kl} e^{i(kt+ls)} \quad (10)$$

and $\|f\|^2 = \sum_{-\infty < k,l < \infty} |c_{kl}|^2 < \infty$, where $c_{kl} = \langle f, e_{kl} \rangle$, $e_{kl}(t,s) = e^{ikt}e^{ils}$. The functions in $L^2(\mathbb{T}^2)$ with $c_{kl} = 0$ for $k < 0$ or $l < 0$ constitute a closed subspace of $L^2(\mathbb{T}^2)$, denoted

$$H^2(\mathbb{T}^2) = \Big\{f \in L^2(\mathbb{T}^2) \mid f(e^{it}, e^{is}) = \sum_{k,l \geq 0} c_{kl} e^{i(kt+ls)}\Big\}. \quad (11)$$

Let $H^2(\mathbb{D}^2)$ be the class of complex holomorphic functions in the poly-disc $\mathbb{D} \times \mathbb{D}$ satisfying

$$\sup_{0 \leq r_1, r_2 < 1} \int_{-\pi}^{\pi} \int_{-\pi}^{\pi} |f(r_1 e^{it}, r_2 e^{is})|^2 dtds < \infty. \quad (12)$$

It is shown in [18] that there exists an isometric isomorphic mapping between $H^2(\mathbb{D}^2)$ and $H^2(\mathbb{T}^2)$. For $f \in L^2(\mathbb{T}^2)$, denote

$$\begin{aligned} f^{+,+}(e^{it}, e^{is}) &= \sum_{k,l \geq 0} c_{kl} e^{i(kt+ls)}, \\ f^{+,-}(e^{it}, e^{is}) &= \sum_{k,-l \geq 0} c_{kl} e^{i(kt+ls)}, \\ f^{-,+}(e^{it}, e^{is}) &= \sum_{-k,l \geq 0} c_{kl} e^{i(kt+ls)}, \\ f^{-,-}(e^{it}, e^{is}) &= \sum_{-k,-l \geq 0} c_{kl} e^{i(kt+ls)}; \end{aligned} \quad (13)$$

and

$$\begin{aligned} F(e^{it}) &= \frac{1}{2\pi} \int_{-\pi}^{\pi} f(e^{it}, e^{is})ds, \\ G(e^{is}) &= \frac{1}{2\pi} \int_{-\pi}^{\pi} f(e^{it}, e^{is})dt. \end{aligned} \quad (14)$$

The partial Hilbert transforms of $f \in L^2(\mathbb{T}^2)$ are defined as

$$H_{(1)}f(e^{it}, e^{is}) = \sum_{-\infty < k,l < \infty} (-i\,\mathrm{sgn}\,k)c_{kl}e^{i(kt+ls)},$$
$$H_{(2)}f(e^{it}, e^{is}) = \sum_{-\infty < k,l < \infty} (-i\,\mathrm{sgn}\,l)c_{kl}e^{i(kt+ls)}, \quad (15)$$

where $H_{(1)}f$ is the Hilbert transform of $f$ with respect to the first variable and $H_{(2)}f$ is the Hilbert transform of $f$ with respect to the second variable.

From now on, we assume that $f \in L^2(\mathbb{T}^2)$ is real-valued. In the case $f^{+,+}$ and $f^{-,-}$ are mutually conjugate to each other and $f^{-,+}$ and $f^{+,-}$ are as well. Taking the notations (13) and (14) into account, denote

$$h(e^{it}, e^{is}) \triangleq f(e^{it}, e^{is}) - F(e^{it}) - G(e^{is}) + c_{00}. \quad (16)$$

We note that the Fourier coefficients $c_{kl}$ of $h$ are equal to zero when $k = 0$ or $l = 0$. The following relations can be verified directly

$$h^{+,+}(e^{it}, e^{is}) = \frac{1}{4}(I + iH_{(2)})(I + iH_{(1)})h \quad (17)$$

and

$$h^{-,+}(e^{it}, e^{is}) = \frac{1}{4}(I + iH_{(2)})(I - iH_{(1)})h. \quad (18)$$

There then follows

$$h(e^{it}, e^{is}) = \left\{h^{+,+}(e^{it}, e^{is})\right\} + \left\{h^{-,+}(e^{it}, e^{is})\right\}$$
$$+ \left\{h^{+,-}(e^{it}, e^{is})\right\} + \left\{h^{-,-}(e^{it}, e^{is})\right\}. \quad (19)$$

We further have

$$h(e^{it}, e^{is}) = 2\mathrm{Re}\left\{h^{+,+}(e^{it}, e^{is})\right\} + 2\mathrm{Re}\left\{h^{-,+}(e^{it}, e^{is})\right\}. \quad (20)$$

From (16) and (20) we finally obtain

$$f(e^{it}, e^{is}) = 2\mathrm{Re}\left\{h^{+,+}(e^{it}, e^{is})\right\} + 2\mathrm{Re}\left\{h^{-,+}(e^{it}, e^{is})\right\}$$
$$+ F(e^{it}) + G(e^{is}) - c_{00}, \quad (21)$$

where $\left[h(e^{-it}, e^{is})\right]^{+,+}(e^{it}, e^{is}) = h^{-,+}(e^{it}, e^{is})$.

The 2D-PUD algorithm for a general real-valued $2D$ image $f$ of finite energy can be outlined as follows. First apply the 2D-PUD algorithm to the Hardy space signal $h^{+,+}$ and $h^{-,+}$. Then apply the 1D-UBD to the 1D signals $F$ and $G$. Finally take the real parts of all the obtained decomposing terms and add them together using (21). The described algorithm shows that 2D-PUD for the 2D Hardy space functions is crucial.

## III. THE 2D PARTIAL UNWINDING DECOMPOSITION (2D-PUD) FOR THE HARDY SPACE FUNCTIONS

The analysis in the last section shows that the 2D-PUD of 2D $L^2$ functions is reduced to that of the related 2D Hardy space functions, and to the related 1D-UBD of some 1D functions.

### A. 2D-PUD on $H^2(\mathbb{D}^2)$

Let $f(z, w) \in H^2(\mathbb{D}^2)$. Then $f^{+,+}(z, w) = f(z, w) = \sum_{k \geq 0, l \geq 0} c_{kl}z^k w^l$, where $\sum_{k \geq 0, l \geq 0} |c_{kl}|^2 < \infty$. The algorithm given in this section does not assume $c_{kl} = 0$ for $k = 0$ or $l = 0$. Set $f_1 = f$. Denote

$$g(z, w) = f_1(z, w) - f_1(z, 0) - f_1(0, w) + f_1(0, 0). \quad (22)$$

Notice that if $z = 0$, then $g(z, w) = 0$ for any $w \in \mathbb{D}$, and if $w = 0$, then $g(z, w) = 0$ for any $z \in \mathbb{D}$. These imply

$$g(z, w) = zwf_2(z, w), \quad (23)$$

where $f_2$ is an $H^2(\mathbb{D}^2)$ function. Thus we obtain

$$f(z, w) = zwf_2(z, w) + f_1(z, 0) + f_1(0, w) - f_1(0, 0), \quad (24)$$

where

$$f_2(z, w) = \frac{f_1(z, w) - f_1(z, 0) - f_1(0, w) + f_1(0, 0)}{zw}. \quad (25)$$

Repeating the same procedure for $f_2(z, w)$, we get

$$f(z, w) = (zw)^2 f_3(z, w) + zw\left[f_2(z, 0) + f_2(0, w) - f_2(0, 0)\right]$$
$$+ f_1(z, 0) + f_1(0, w) - f_1(0, 0), \quad (26)$$

where

$$f_3(z, w) = \frac{f_2(z, w) - f_2(z, 0) - f_2(0, w) + f_2(0, 0)}{zw}. \quad (27)$$

Repeating this process up to N-times, we have

$$f(z, w) = \sum_{m=1}^{N} (zw)^{m-1}\left[f_m(z, 0) + f_m(0, w) - f_m(0, 0)\right]$$
$$+ (zw)^N f_{N+1}(z, w), \quad (28)$$

where

$$f_{m+1}(z, w) = \frac{f_m(z, w) - f_m(z, 0) - f_m(0, w) + f_m(0, 0)}{zw}. \quad (29)$$

By denoting

$$S_N(f)(z, w) = \sum_{m=1}^{N} (zw)^{m-1}\left[f_m(z, 0) + f_m(0, w) - f_m(0, 0)\right] \quad (30)$$

and

$$R_N(f)(z, w) = (zw)^N f_{N+1}(z, w), \quad (31)$$

where $f_{N+1}$ is an $H^2(\mathbb{D}^2)$ function, we obtain

$$f(z, w) = S_N(f)(z, w) + R_N(f)(z, w). \quad (32)$$

Denote the 2D classical Fourier series $(N - 1)$-partial sum decomposition by

$$f(z, w) = \widetilde{S}_N(f)(z, w) + \widetilde{R}_N(f)(z, w), \quad (33)$$

where $\widetilde{S}_N(f)(z, w) = \sum_{0 \leq k,l \leq N-1} c_{kl}z^k w^l$. It is well known that $\|\widetilde{R}_N(f)\|^2 = \sum_{k \text{ or } l \geq N} |c_{kl}|^2 \to 0$. Fig. 2 shows that $\widetilde{R}_N(f)$ spreads over the region I ∪ II ∪ III; while $R_N(f)$ spreads over only the region II. In below, we show that $S_N(f)$ rapidly converges to $f$ in the $L^2$-norm. Furthermore, if $f$ can
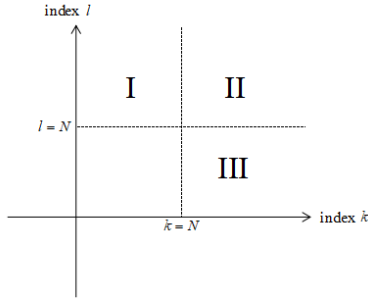
Fig. 2. The energy distribution regions of $R_N(f)$ and $\widetilde{R}_N(f)$.

be holomorphically extended to outside of the closed unit poly-disc, then the exponential decay rate can be attained.

**Theorem 1.** *If $f(z,w) \in H^2(\mathbb{D}^2)$. Then*

$$\|f - S_N(f)\| \to 0, \ N \to \infty. \tag{34}$$

*Moreover, if $f$ can be holomorphically continued to $(1+\delta_1)\mathbb{D} \times (1+\delta_2)\mathbb{D} = \left\{ (z,w) \ \big| \ |z| < 1+\delta_1 \ and \ |w| < 1+\delta_2 \right\}, \ \delta_i > 0, \ i = 1, 2$, then the $L^2$-norm of the remainder $R_N(f)$ decays exponentially.*

*Proof:* Due to the uniqueness of power series expansion of a holomorphic function, $R_N(f)$ is equal to the sum of the power series entries $c_{kl} z^k w^l$ with both $k \geq N$ and $l \geq N$. The energy of $R_N(f)$ is the square sum of the norms of the Fourier coefficients indexed by the integer pairs in the region II in Fig. 2, that is, $\|f - S_N(f)\|^2 = \sum\limits_{k \geq N, l \geq N} |c_{kl}|^2 \to 0, \ N \to \infty$. In addition, let $f(z,w) \in H^2(\mathbb{D}^2)$ be holomorphically continued to $(1+\delta_1)\mathbb{D} \times (1+\delta_2)\mathbb{D}, \ \delta_i > 0, \ i = 1, 2$. Letting $\beta_1 = 1 + \frac{\delta_1}{2}$ and $\beta_2 = 1 + \frac{\delta_2}{2}$, we have $c_{kl} \beta_1^k \beta_2^l \to 0$ for either $k \to \infty$ or $l \to \infty$. So there exists $M_1 > 0$ such that $|c_{kl}| < \frac{M_1}{\beta_1^k \beta_2^l}$ for any $k \geq 0$ and $l \geq 0$. This induces $\|f - S_N(f)\|^2 \leq \sum\limits_{k \geq N, l \geq N} \frac{M_1^2}{\beta_1^{2k} \beta_2^{2l}} = M_1^2 \frac{1}{\beta_1^{2N} \beta_2^{2N}} \frac{\beta_2^2}{\beta_2^2 - 1} \frac{\beta_1^2}{\beta_1^2 - 1}$. Thus

$$\|f - S_N(f)\| \leq C_1 a_1^N, \tag{35}$$

where $C_1 = \frac{M_1 \beta_1 \beta_2}{\sqrt{(\beta_1^2 - 1)(\beta_2^2 - 1)}}$ and $a_1 = \frac{1}{\beta_1 \beta_2} < 1$, as desired. ∎

From the iterative process of the function $f$ in $H^2(\mathbb{D}^2)$, $f_m(z,w)$ belongs to $H^2(\mathbb{D}^2)$ for every $m \geq 1$. This implies that the univariate complex functions $f_m(z,0)$ and $f_m(0,w)$ belong to $H^2(\mathbb{D})$, respectively. By using the 1D-UBD, each $f_m(z,0)$ and $f_m(0,w)$ can be approximated by an infinite linear combination of Blaschke products. In summary, for an arbitrary function in $H^2(\mathbb{D}^2)$, we obtain the 1D-UBD based 2D-PUD. Combining the iterative processes (7) and (28), we get the 2D partial unwinding system consisting of $\left\{ (zw)^{m-1} \right\}_{m=1}^{\infty}$, $\left\{ (zw)^{l-1} z \prod\limits_{k=1}^{\infty} \frac{z - a_{kl}}{1 - \overline{a_{kl}} z} \right\}_{l=1}^{\infty}$ and $\left\{ (zw)^{j-1} w \prod\limits_{k=1}^{\infty} \frac{w - b_{kj}}{1 - \overline{b_{kj}} w} \right\}_{j=1}^{\infty}$. Due to the adaptivity of the 1D-UBD, the 2D partial unwinding system is adaptive. In fact, different elements in the system are mutually orthogonal.

**Theorem 2.** *If $f(z,w) \in H^2(\mathbb{D}^2)$. Then its 2D partial unwinding system is orthornormal.*

*Proof:* Without loss of generality, set $l \geq j$. Let $B_1(z) = \prod\limits_{k=1}^{\infty} \frac{z - a_{kl}}{1 - \overline{a_{kl}} z}$, $B_2(w) = \prod\limits_{k=1}^{\infty} \frac{w - b_{kj}}{1 - \overline{b_{kj}} w}$. Then

$$\left\langle (zw)^{l-1} z \prod_{k=1}^{\infty} \frac{z - a_{kl}}{1 - \overline{a_{kl}} z}, (zw)^{j-1} w \prod_{k=1}^{\infty} \frac{w - b_{kj}}{1 - \overline{b_{kj}} w} \right\rangle$$

$$= \frac{1}{4\pi^2} \int_{-\pi}^{\pi} \int_{-\pi}^{\pi} (e^{it})^{l-j+1} B_1(e^{it}) \overline{(e^{is})^{j-l+1} B_2(e^{is})} dt ds$$

$$= \frac{1}{2\pi} \int_{-\pi}^{\pi} (e^{it})^{l-j+1} B_1(e^{it}) dt \cdot \overline{\frac{1}{2\pi} \int_{-\pi}^{\pi} (e^{is})^{j-l+1} B_2(e^{is}) ds}.$$

From Cauchy's theorem, we have

$$\int_{|\xi|=r} \xi^{l-j} B_1(\xi) d\xi = 0, \ \text{i. e.,} \ \int_{-\pi}^{\pi} (e^{it})^{l-j+1} B_1(re^{it}) dt = 0,$$

where $0 < r < 1$. As the modulus of a Blaschke product in the unit disc is less than 1, it is seen from Lebesgue's dominated convergence theorem that

$$\lim_{r \to 1^-} \int_{-\pi}^{\pi} (e^{it})^{l-j+1} B_1(re^{it}) dt = \int_{-\pi}^{\pi} (e^{it})^{l-j+1} B_1(e^{it}) dt = 0.$$

This gives the zero value to the above inner product. The orthogonality between the other different functions in the 2D partial unwinding system can be similarly proved. Moreover, due to the unit modulus property of Blaschke products on the unit circle [32], the norm of each function in the system is 1. The proof of the theorem is thus complete. ∎

### B. 2D-PUD on $L^2(\mathbb{T}^2)$ Images

The principle of the 2D-PUD algorithm for $L^2$ image functions is studied in Subsection II-B through reducing the $L^2$ to the $H^2$ cases. In this subsection we aim at the implementation of the algorithm. Any image denoted as $I(x,y)$ ($x = 1, 2, \cdots, m, \ y = 1, 2, \cdots, n$ with size $m \times n$) can be considered as discrete values of a real function $f(e^{it}, e^{is})$ in $L^2(\mathbb{T}^2)$. Preprocess $f$ to obtain $h$ by throwing away the terms $c_{kl}$ of $f$ for $k = 0$ or $l = 0$, and then find the boundary limits of the functions $h^{+,+}$ and $h^{-,+}$ through the partial Hilbert transforms (15). The Nevenlinna decompositions of $h^{+,+}$ and $h^{-,+}$ and the consecutive ones pursuing the 1D-UBD are all done on the boundaries $\{|z| = 1\}$ or $\{|w| = 1\}$, and adopt the finite Blaschke decomposition method given in [35]. As proved in the previous section, the obtained 2D-PUD generates an adaptive fast converging orthonormal system.

The flowchart of the 2D-PUD is shown in Fig. 3. First, an input 2D image $f$ is preprocessed to obtain $h$ from (16). Next, the respective 1D-UBD results of 1D signals $F$ and $G$ are computed. Then, $h$ is decomposed to get $h^{+,+}$ and $h^{-,+}$ from (17) and (18), respectively. After that, we apply Algorithm 1 and Algorithm 2 to get the approximation results $u^N$ and $v^N$ of $h^{+,+}$ and $h^{-,+}$, respectively. Finally, taking the equations (16) and (21) into consideration, we get the approximation result $f^N$. Thus, the 2D-PUD algorithm is achieved.

The computational complexity of 2D-PUD is calculated as follows. Assume that the image size is $L \times L$.

- Since the calculation of Hilbert transform is obtained by fast Fourier transform (FFT) [38], the complexities of
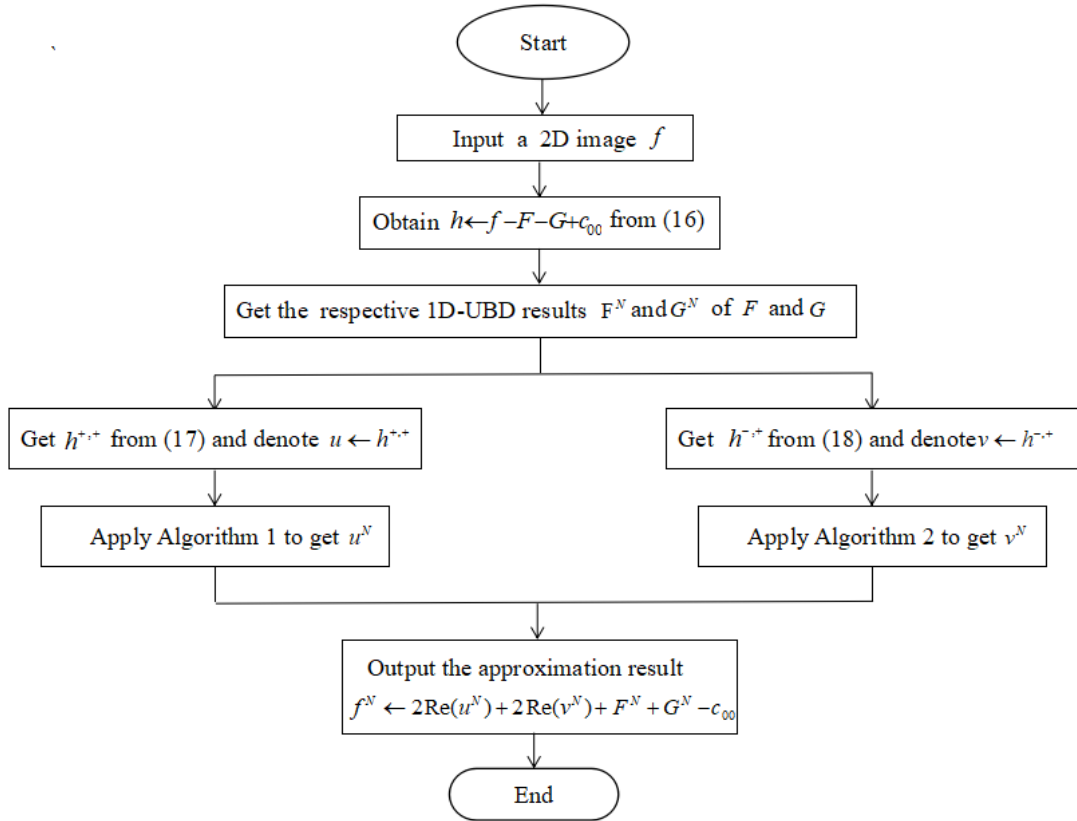
Fig. 3.  The flowchart of 2D-PUD on image decomposition with level $N$.

---

**Algorithm 1** 2D-PUD of $u$

**Input:** 2D signal $u$ and decomposition level $N$.
**Output:** approximation result $u^N$.

1:  Initialize $u_1 = u$ and $u^N = 0$.
2:  **for** $k = 1$ to $N$ **do**
3:      Get $u_k(e^{it}, 0)$, $u_k(0, e^{is})$ and $u_k(0,0)$ from (14);
4:      Get $T_k = (e^{it}e^{is})^{k-1}$ and choose 1D unwinding decomposition level $n$;
5:      Get the 1D unwinding decomposition $u_k^n(e^{it}, 0)$ of $u_k(e^{it}, 0)$ and $u_k^n(0, e^{is})$ of $u_k(0, e^{is})$ from reference [35];
6:      Get $u^N = u^N + T_k[u_k^n(e^{it}, 0) + u_k^n(0, e^{is}) - u_k(0,0)]$ from (30);
7:      Get $u_{k+1} = [u_k - u_k(e^{it}, 0) - u_k(0, e^{is}) + u_k(0,0)]/(e^{it}e^{is})$ from (29);
8:  **end for**
9:  **return** $u^N$.

---

**Algorithm 2** 2D-PUD of $v$

**Input:** 2D signal $v$ and decomposition level $N$.
**Output:** approximation result $v^N$.

1:  Initialize $v_1 = v$ and $v^N = 0$.
2:  **for** $k = 1$ to $N$ **do**
3:      Get $v_k(e^{-it}, 0)$, $v_k(0, e^{is})$, and $v_k(0,0)$ from (14);
4:      Get $I_k = (e^{-it}e^{is})^{k-1}$ and select 1D unwinding decomposition level $n$;
5:      Get the 1D unwinding decomposition $v_k^n(e^{it}, 0)$ of $\overline{v_k(e^{-it}, 0)}$ and $v_k^n(0, e^{is})$ of $v_k(0, e^{is})$ from reference [35];
6:      Get $v^N = v^N + I_k[\overline{v_k^n(e^{it}, 0)} + v_k^n(0, e^{is}) - v_k(0,0)]$;
7:      Get $v_{k+1} = [v_k - v_k(e^{-it}, 0) - v_k(0, e^{is}) + v_k(0,0)]/(e^{-it}e^{is})$;
8:  **end for**
9:  **return** $v^N$.

---

the projection signals $f^{+,+}$ and $f^{-,+}$ are $\mathcal{O}(L^2 \log L)$, respectively.

- The respective complexities of computing the zeros of finite Blaschke product of step 5 in both Algorithm 1 and Algorithm 2 are $\mathcal{O}(ML)$ [39], respectively, where $M$ is the number of discrete points in the unit disc $\mathbb{D}$.
- The computational complexities of step 6 in both Algorithm 1 and Algorithm 2 are $\mathcal{O}(L^2)$, respectively.

Therefore, the computational complexity of the 2D-PUD algorithm is $\mathcal{O}(L^2 \log L)$, which is the same as that of two-dimensional fast Fourier transform (2D-FFT).

## IV. EXPERIMENTAL RESULTS

Two sets of the experiments are conducted to demonstrate the effectiveness and efficiency of the proposed approach. We use the following naming pattern: slice-1D-AFD and slice-1D-UBD represent that the image is processed row-by-row by applying 1D-UBD and 1D-AFD, respectively. 2D-GA stands 2D greedy algorithm (or match pursuit) [26]–[31] on the product-Szegö dictionary. 2D-FS and 2D-PUD denotes 2D

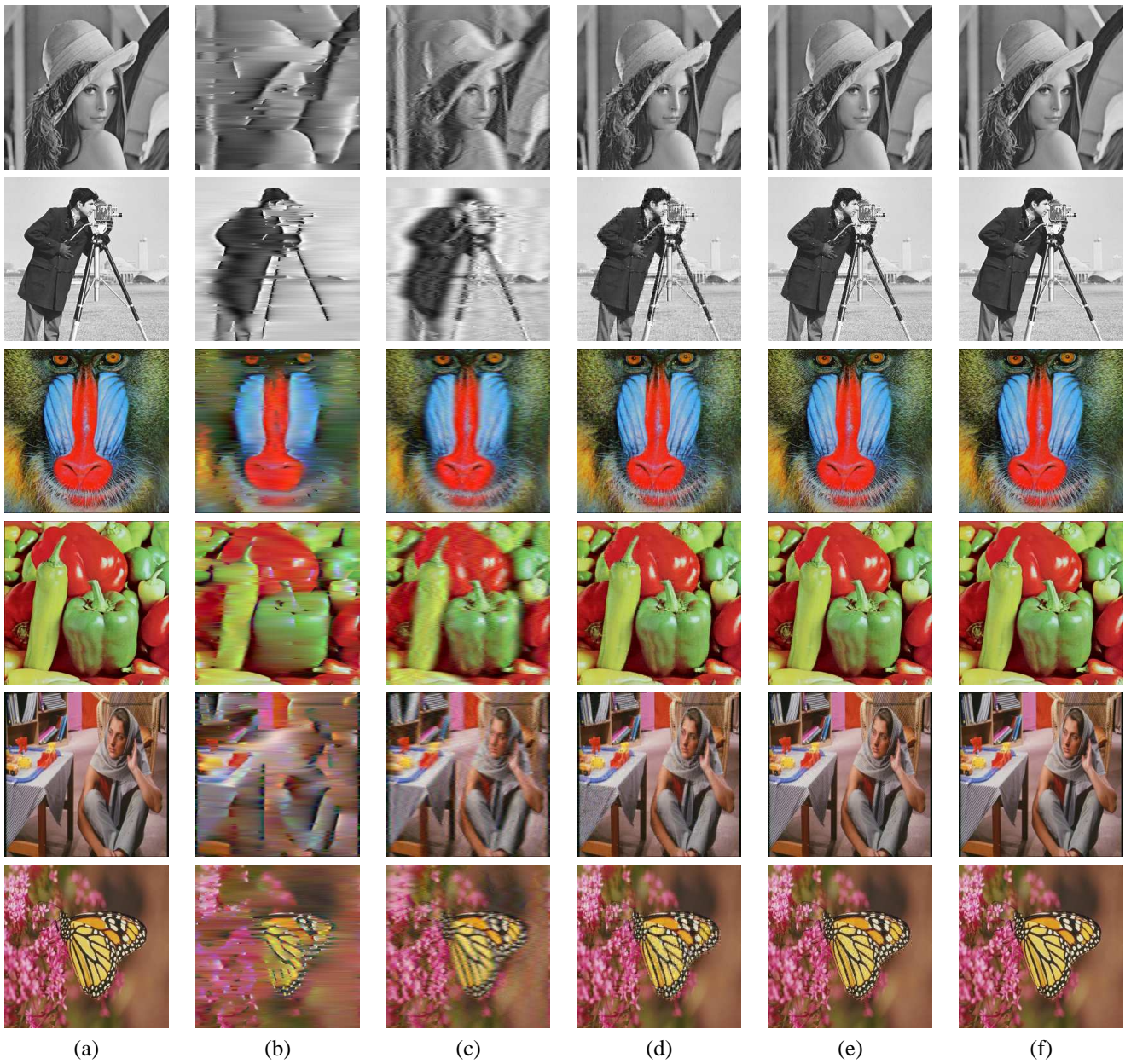|     |     |     |     |     |     |
| --- | --- | --- | --- | --- | --- |
| (a) | (b) | (c) | (d) | (e) | (f) |

Fig. 4.   Comparison of the different algorithms with decomposition level $N = 5$. (a) Original image, (b) slice-1D-AFD, (c) slice-1D-UBD, (d) 2D-GA, (e) 2D-FS, and (f) 2D-PUD.
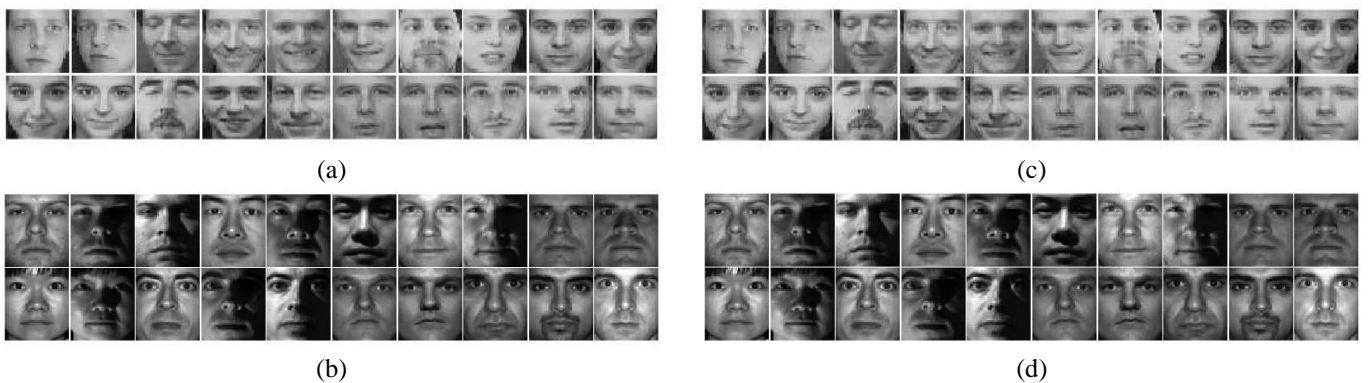


Fig. 5.   Experimental results on image reconstruction. (a). 20 original images from ORL face database. (b). 20 original images from Yale face database. (c). Image reconstruction results of (a) by 2D-PUD with N=5. (d). Image reconstruction results of (b) by 2D-PUD with N=5.

Fourier series and our proposed approach, respectively. We implement the 2D decompositions by adopting overlapping block methods. The first set of our experiments compares the efficiency of the image decomposition and reconstruction among slice-1D-AFD, slice-1D-UBD, 2D-GA, 2D-FS, and our proposed 2D-PUD on 6 popular test images and two large databases - The ORL Database of Faces and Yale Face Database, including 240 grayscale images from ORL and 1026 grayscale images from Yale, respectively. The second set of experiments illustrates the effectiveness of our proposed algorithm by the application in watermarking through comparing it with the popular discrete cosine transform (DCT) based watermarking technique. Some commonly used attacks are also tested, including Gaussian filtering, salt and pepper noise, and image cutting.

## A. Image Decomposition and Reconstruction

We use the following measurements to evaluate the reconstruction quality of images: peak signal-to-noise rate (PSNR), structural similarity index (SSIM), edge intensity (EI), and figure definition (FD).

PSNR is defined as

$$\text{PSNR} = 10 \log \frac{255^2}{\text{MSE}}, \quad (36)$$

where

$$\text{MSE} = \frac{1}{m \times n} \sum_{x=1}^{m} \sum_{y=1}^{n} [\text{I}(x,y) - \text{J}(x,y)]^2, \quad (37)$$

$m \times n$ is the size of grayscale image I. J is the reconstructed image of I.

SSIM [40] measures the structural similarity between the original image I and the reconstructed image J. Based on the calculation of the luminance, the contrast and the structural correlation of images, SSIM is computed by

$$\text{SSIM}(\text{I}, \text{J}) = [l(\text{I}, \text{J})]^\alpha [c(\text{I}, \text{J})]^\beta [s(\text{I}, \text{J})]^\gamma, \quad (38)$$

where $l(\text{I}, \text{J}) = (2\mu_\text{I}\mu_\text{J} + C_1)/(\mu_\text{I}^2 + \mu_\text{J}^2 + C_1)$ represents the luminance of images. $c(\text{I}, \text{J}) = (2\sigma_\text{I}\sigma_\text{J} + C_2)/(\sigma_\text{I}^2 + \sigma_\text{J}^2 + C_2)$ compares the contrast of images. $s(\text{I}, \text{J}) = (\sigma_\text{IJ} + C_3)/(\sigma_\text{I}\sigma_\text{J} + C_3)$ measures the structural correlation of images, where $\mu_\text{I}$, $\mu_\text{J}$, $\sigma_\text{I}$, $\sigma_\text{J}$, and $\sigma_\text{IJ}$ are the local means, standard deviations, and cross-covariance for the images I and J. In this article, $\alpha = \beta = \gamma = 1$ and $C_3 = C_2/2$. Larger PSNR and SSIM values usually correspond to better reconstruction quality.

EI [41] is the average sum of the absolute value of the image edges.

FD [41] reflects the clarity of an image, computed as

$$\text{FD} = \frac{\sum_{x=1}^{m-1} \sum_{y=1}^{n-1} \left[ \frac{[I(x+1,y)-I(x,y)]^2 + [I(x,y+1)-I(x,y)]^2}{2} \right]^{\frac{1}{2}}}{(m-1) \times (n-1)}, \quad (39)$$

where $m \times n$ is the size of image I. The difference of the EI and FD values between the original image and the reconstructed image also represent the reconstruction quality. The smaller the difference is, the higher the reconstruction quality will be.

The above criteria, namely, PSNR, SSIM, EI, and FD, can be directly used for evaluating the grayscale images. For color images, we calculate the average of the respective PSNR, SSIM, EI, and FD values of three different color channels. Regardless of color or grayscale images, better reconstruction qualities are indicated by larger values of PSNR and SSIM, and smaller difference of EI and FD.

### TABLE I
### THE EI AND FD VALUES OF THE ORIGINAL IMAGES.

| Criteria | Lena | Cameraman | Baboon | Peppers | Barbara | Monarch | ORL | Yale |
|---|---|---|---|---|---|---|---|---|
| EI | 0.2579 | 0.3186 | 0.4267 | 0.2688 | 0.3586 | 0.3653 | 0.4755 | 0.3597 |
| FD | 0.0305 | 0.0464 | 0.0667 | 0.0297 | 0.0469 | 0.0418 | 0.0545 | 0.0190 |

### TABLE II
### COMPARISON RESULTS AMONG FIVE DECOMPOSITION APPROACHES ON PSNR, SSIM, EI, AND FD VALUES OF THE SELECTED SIX IMAGES AND RESPECTIVE AVERAGES OF ORL AND YALE DATABASES. THE DECOMPOSITION LEVEL IS $N = 5$.

| Images | Methods | PSNR | SSIM | EI | FD |
|---|---|---|---|---|---|
| Lena | Slice-1D-AFD | 20.6606 | 0.5331 | 0.1799 | 0.0195 |
| | Slice-1D-UBD | 23.7143 | 0.6731 | 0.2440 | 0.0298 |
| | 2D-GA | 30.5142 | 0.9221 | 0.2538 | 0.0309 |
| | 2D-FS | 34.4962 | 0.9549 | 0.2562 | 0.0313 |
| | 2D-PUD | **52.1189** | **0.9985** | **0.2580** | **0.0307** |
| Cameraman | Slice-1D-AFD | 20.1428 | 0.5844 | 0.2296 | 0.0279 |
| | Slice-1D-UBD | 19.4296 | 0.5720 | 0.2533 | 0.0331 |
| | 2D-GA | 26.2435 | 0.8839 | 0.3222 | 0.0446 |
| | 2D-FS | 28.8802 | 0.9232 | 0.3200 | 0.0631 |
| | 2D-PUD | **48.4741** | **0.9966** | **0.3198** | **0.0467** |
| Baboon | Slice-1D-AFD | 20.4109 | 0.3910 | 0.2392 | 0.0307 |
| | Slice-1D-UBD | 22.4272 | 0.5862 | 0.3100 | 0.0412 |
| | 2D-GA | 26.5681 | 0.8474 | 0.3938 | 0.0565 |
| | 2D-FS | 29.6990 | 0.9278 | 0.4150 | 0.0817 |
| | 2D-PUD | **49.1860** | **0.9987** | **0.4273** | **0.0668** |
| Peppers | Slice-1D-AFD | 21.4408 | 0.5932 | 0.2356 | 0.0259 |
| | Slice-1D-UBD | 22.5868 | 0.6364 | 0.2577 | 0.0305 |
| | 2D-GA | 31.0335 | 0.9285 | 0.2719 | 0.0317 |
| | 2D-FS | 34.7850 | 0.9566 | 0.2683 | 0.0347 |
| | 2D-PUD | **47.9617** | **0.9970** | **0.2701** | **0.0301** |
| Barbara | Slice-1D-AFD | 19.4638 | 0.4295 | 0.2468 | 0.0281 |
| | Slice-1D-UBD | 22.7953 | 0.6222 | 0.3059 | 0.0365 |
| | 2D-GA | 28.9639 | 0.8973 | 0.3459 | 0.0427 |
| | 2D-FS | 32.2859 | 0.9458 | 0.3542 | 0.0560 |
| | 2D-PUD | **44.7746** | **0.9962** | **0.3621** | **0.0477** |
| Monarch | Slice-1D-AFD | 19.7792 | 0.5743 | 0.2408 | 0.0296 |
| | Slice-1D-UBD | 21.5031 | 0.6821 | 0.2944 | 0.0356 |
| | 2D-GA | 26.5390 | 0.9211 | 0.3552 | 0.0445 |
| | 2D-FS | 32.2859 | 0.9559 | 0.3599 | 0.0486 |
| | 2D-PUD | **50.8838** | **0.9983** | **0.3659** | **0.0421** |
| ORL | Slice-1D-AFD | 18.1445 | 0.2945 | 0.3679 | 0.0156 |
| | Slice-1D-UBD | 18.7004 | 0.3633 | 0.3988 | 0.0334 |
| | 2D-GA | 27.8298 | 0.8871 | 0.4703 | 0.0679 |
| | 2D-FS | 30.1065 | 0.9224 | 0.4648 | 0.0728 |
| | 2D-PUD | **41.8766** | **0.9944** | **0.4772** | **0.0597** |
| Yale | Slice-1D-AFD | 17.0724 | 0.3356 | 0.2859 | 0.0421 |
| | Slice-1D-UBD | 17.4353 | 0.3796 | 0.3042 | 0.0454 |
| | 2D-GA | 30.2005 | 0.9259 | 0.3614 | 0.0407 |
| | 2D-FS | 34.1292 | 0.9593 | 0.3568 | 0.0418 |
| | 2D-PUD | **45.0382** | **0.9935** | **0.3600** | **0.0385** |

To show the efficiency of the proposed algorithm, we conduct a number of experiments. First, six popular test images, including two grayscale and four color images of size $256 \times 256$, are selected as original images. Fig. 4(a) lists the six original images that are respectively "lena", "cameraman",
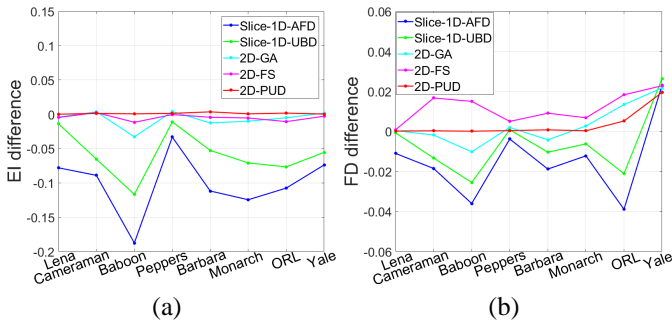
Fig. 6. Comparison results of (a) EI and (b) FD differences on six test images and respective averages of ORL and Yale databases among five methods with the decomposition level $N = 5$.



Fig. 7. Comparison results of the proposed 2D-PUD with different decomposition levels on (a) PSNR, (b) SSIM, (c) EI, and (d) FD for image "lena".

"baboon", "peppers", "barbara", and "monarch". The reconstructed images through the tested five algorithms with $N = 5$ are displayed in Fig. 4(b)-(f). In Fig. 4 we can see that our proposed approach demonstrates best visual performance on the six test images. Then, we conduct the experiments on two face databases. These face images are shot at different times, with different lighting, expressions and facial details. We compare separately the average PSNR, SSIM, EI, and FD values for each database. To demonstrate the construction quality visually, 20 images from each of above two databases and their corresponding reconstruction images through our proposed approach are illustrated in Fig. 5. The results show that the reconstructed images are visually indistinguishable from the corresponding original images.

Table I lists the EI and FD values of the six original images and the average EI and FD values of the ORL and Yale databases, respectively. Tables II gives the comparison results of the PSNR, SSIM, EI, and FD values of the six images and respective averages of the ORL and Yale databases among the five methods with $N = 5$. Fig. 6 compares the EI and FD differences of the six images and respective averages of the ORL and Yale databases among the five approaches with $N = 5$. Table II illustrates that our proposed approach outperforms other approaches on all test images. Fig. 6 shows that 2D-PUD has the smallest differences of EI and FD among the five methods.

To further show the effect of the decomposition level, the comparison results of the PSNR, SSIM, EI, and FD values of the reconstructed "lena" with different decomposition levels among five tested algorithms are shown in Fig. 7. In Fig. 7(c) and (d), black dotted lines represent the EI and FD values of the original image. Clearly, as the decomposition level $N$ increases, the PSNR and SSIM values of the reconstructed image become larger, and the differences of the EI and FD values between the original image and the reconstructed image become smaller. According to Fig. 7(a), the PSNR and SSIM values of the 2D-PUD with $N = 1$ are already larger than the respective PSNR and SSIM values of the slice-1D-AFD and slice-1D-UBD with $N = 5$. Besides, when $N$ increases, the PSNR value of the 2D-PUD is remarkably larger than those of the 2D-GA and 2D-FS.
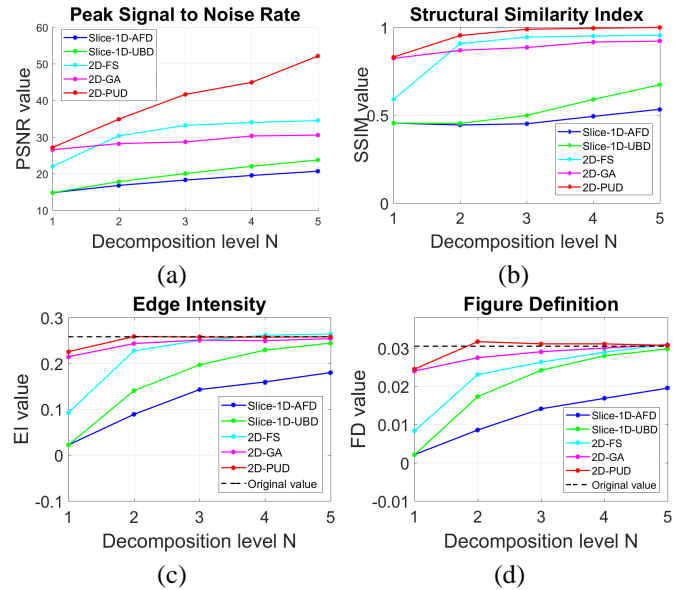
## B. Application in Digital Watermarking

There are various schemes to embed and extract the watermark. They can be divided into two categories. One is that the watermark is embedded in the spatial domain and the other is that it is embedded in the transform domain. In the spatial domain, the watermark is directly embedded into a host image by modifying the pixel values [42]–[45]. In the transform domain, the coefficients of the transformed host image are modified [46]–[49]. The popular transform domain techniques include two-dimensional discrete cosine transform (2D-DCT), two-dimensional discrete Fourier transform, etc. Spatial domain techniques have lower computational complexity, but are less robust than the transform domain techniques [46]. 2D-PUD generates an adaptive orthonormal system that can offer a more secure watermark embedding in the transform domain, as the decomposing components of the watermarked image are different from those of the original image due to the adaptivity. We outline the specific approach as follows.

Assume that the pixels of a host image and a watermark are discrete values of functions $f$ and $g$ in $L^2(\mathbb{T}^2)$, respectively. Then $f^{+,+}$ and $f^{-,+}$, as well as $g^{+,+}$ and $g^{-,+}$, can be easily obtained through the partial Hilbert transforms described in Subsection II-B. From Theorem 2, $f^{+,+}$ produces an adaptive orthonormal system. Due to the orthogonality of the 2D partial unwinding system, $g^{+,+}$ can be projected into the system. Similarly, $g^{-,+}$ can also be projected into the 2D partial unwinding orthonormal system of $f^{-,+}$. As a result, taking the relations among $g^{+,+}, g^{-,+}$, and $g$ into consideration, the original watermark is scrambled by the 2D partial unwinding orthonormal system of the host image to obtain a new watermark. There is a difference between the original watermark $g$ and the projected watermark $\overline{g}$. This difference will be recorded separately and added back to the extracted projected watermark during the final extraction.

Algorithm 3 illustrates how 2D-PUD is applied to the

**Algorithm 3** The watermark embedding and extraction processes using 2D-PUD method

---

**Input:** An original host image $\mathbf{I}$ of size $m \times n$, an original watermark $\mathbf{A}$ of size $p \times q$ ($p \leq m, q \leq n$), a small positive embedding factor $c$.

**Output:** The watermarked image $\mathbf{J}$ and extracted watermark $\overline{\mathbf{A}}$.

1: Choose the decomposition level $N$ to obtain the reconstructed image $\mathbf{I_1}$ by using the 2D-PUD method.
2: Get a new watermark $\mathbf{A_1}$ by projecting the original watermark $\mathbf{A}$ into the 2D partial unwinding orthonormal system of $\mathbf{I}$.
3: Randomly embed the watermark $\mathbf{A_1}$ through the process $\mathbf{I_1} + c\mathbf{A_1}$ to get the watermarked image $\mathbf{J}$ and save the embedded positions.
4: Extract the watermark $\overline{\mathbf{A}}$ by the process $\mathbf{A}\text{-}\mathbf{A_1}+(\mathbf{J}\text{-}\mathbf{I}_1)/c$ at the embedded positions.

---
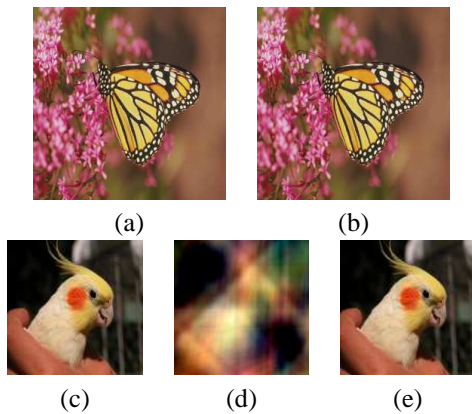


(a)    (b)

(c)    (d)    (e)

Fig. 8. Embedding and extraction of the watermark image "bird" using 2D-PUD method without attacks. (a) Original host image "monarch", (b) the watermarked image, (c) original watermark "bird", (d) the projected watermark, and (e) the extracted watermark.

watermark embedding and extraction processes. In order to test the efficiency of our proposed watermarking technique, PSNR and normalized correlation coefficient (NCC) [49] are used to assess the similarity, in which PSNR is used to assess the similarity between the host images and the watermarked images, while NCC is used to assess the similarity between the original watermark $\mathbf{A}$ and the extracted watermark $\overline{\mathbf{A}}$. NCC is computed as follows:

$$\text{NCC} = \frac{\sum\limits_{x=1}^{p}\sum\limits_{y=1}^{q}[\mathbf{A}(x,y) \times \overline{\mathbf{A}}(x,y)]}{\sqrt{\sum\limits_{x=1}^{p}\sum\limits_{y=1}^{q}\mathbf{A}(x,y)^2}\sqrt{\sum\limits_{x=1}^{p}\sum\limits_{y=1}^{q}\overline{\mathbf{A}}(x,y)^2}}. \qquad (40)$$

For color images, average PSNR and NCC values are computed from three different color channels. Larger PSNR and NCC values indicate better embedding and watermark extraction results, respectively.

As described in the previous subsection, 2D-PUD with the decomposition level $N = 5$ has high reconstruction quality, we choose $N = 5$ in Algorithm 3. In addition, the small positive embedding factor $c$ in Algorithm 3 is selected as

$10^{-1}$. Fig. 8 shows the embedding and extraction of the watermark image "bird" using the 2D-PUD method. As shown in Fig. 8 (a) and (c), the color image "monarch" ($256 \times 256$) is used as the host image and another color image "bird" ($128 \times 128$) is chosen as the watermark. Fig. 8 (d), (b), and (e) display the projected watermark, the watermarked image, and the extracted watermark, respectively. There is no visible differences either between the host and watermarked images, or between the original and extracted watermark images. The PSNR value between the watermarked and the original host images is 34.7994, and the NCC value between the original and the extracted watermarks is 1, which indicate both the embedding and extraction results are promising.

TABLE III
COMPARISON OF THE NCC VALUES BETWEEN 2D-DCT AND 2D-PUD METHODS UNDER DIFFERENT ATTACKS.

| Attacks | 2D-DCT | 2D-PUD |
|---|---|---|
| Gaussian filtering (3,0.3) | 0.9997 | **0.9998** |
| Salt and pepper noise 0.001 | 0.7075 | **0.9447** |
| Cutting (8,8) | 0.7361 | **0.9510** |

TABLE IV
COMPARISON OF THE EXTRACTED WATERMARKS BETWEEN 2D-DCT AND 2D-PUD METHODS UNDER DIFFERENT ATTACKS.

| Attacks | Gaussian filtering (3,0.3) | Salt and pepper noise 0.001 | Cutting (8,8) |
|---|---|---|---|
| 2D-DCT | | | |
| 2D-PUD | | | |



The robustness of our method is compared with popular 2D-DCT based watermarking technique, which algorithm is briefly described as follows. (i) Perform 2D-DCT on the host image $\mathbf{I}$ to obtain the transformed image $\widehat{\mathbf{I}}$. (ii) Randomly embed the original watermark $\mathbf{A}$ by multiplying the above same small positive number $c$ to obtain the image $\widehat{\mathbf{I}} + c\mathbf{A}$ and save the embedded positions. (iii) Implement 2D inverse discrete cosine transform (2D-IDCT) on the above image to get the watermarked image $\mathbf{J}=(\widehat{\mathbf{I}} + c\mathbf{A})^{\vee}$. (iv) Extract the watermark through the process $(\widehat{\mathbf{J}} - \widehat{\mathbf{I}})/c$ at the embedded positions.

Table III compares the NCC values between 2D-DCT and 2D-PUD under three attacks, which are respectively Gaussian filtering with $3 \times 3$ filter size, salt and pepper noise 0.001, and image cutting with $8 \times 8$ block size. In Table III, we can see that our proposed approach performs much better on salt and pepper noise and image cutting attacks than 2D-DCT. Comparison of the extracted watermark images between the 2D-DCT and 2D-PUD methods under the above attacks is

shown in Fig. IV. Our approach also visually performs much better under above two attacks than 2D-DCT.

The experimental results demonstrate the robustness of our proposed approach in digital watermarking. The main reason is that the watermark embedded by our method is the projected watermark by the 2D partial unwinding orthonormal system of the host image and the remaining part after the projection is recorded separately. Since attacks are applied on the watermarked images, that is, only part of the watermark is affected by the attacks in our approach. On the contrary, the whole watermark is affected by the attacks in 2D-DCT method. This is due to the fact that our approach decomposes different images into different decomposition components adaptively, while the discrete cosine transform use the same basis.

## V. Conclusions and Future Works

In this paper, the novel 2D non-linear phase decomposition algorithm 2D-PUD is proposed. The matlab code without optimization (we will do the optimization soon) is provided in the link: http://www.fst.umac.mo/en/staff/fsttq.html. The decomposition generates an adaptive orthonormal system. Its convergence is obviously much faster than the standard Fourier methods. So, theoretically anywhere when the Fourier methods can be used, this new method can be used with much more effectiveness and efficiency. As in the 1D case, the proposed method provides the tensor form positive instantaneous phase derivatives that lay foundation in image signal frequency analysis. The experiments illustrate that the proposed method is more efficient in image reconstruction than the standard greedy algorithm and the most commonly used methods in the Fourier category. Apart from the non-linear phase decomposition of images, as an application, the proposed method is more effective in watermarking than the standard discrete cosine transform based watermarking technique. This is due to the fact that our approach decomposes different images into different decomposition components adaptively, while for all images the discrete cosine transform use the same basis. Further applications in image analysis and positive non-linear frequency analysis are to be explored.

## Acknowledgments

## References

[1] Q. Wang, O. Ronneberger, and H. Burkhardt, "Rotational invariance based on Fourier analysis in polar and spherical coordinates," *IEEE Trans. Pattern Anal. Mach. Intell.*, vol. 31, no. 9, pp. 1715-1722, 2009.

[2] Q. Sabatier, S. Ieng, and R. Benosman, "Asynchronous event-based Fourier analysis," *IEEE Trans. on Signal Process.*, vol. 26, no. 5, pp. 2192-2202, 2017.

[3] J. Kim, J. Kim, and C. Kim, "Adaptive image and video retargeting technique based on Fourier analysis," *Proc. IEEE Conf. Comput. Vis. Pattern Recognit.*, 2009, pp. 1730-1737.

[4] P. Chazal, J. Flynn, and R. Reilly, "Automated processing of shoeprint images based on the Fourier transform for use in forensic science," *IEEE Trans. Pattern Anal. Mach. Intell.*, vol. 27, no. 3, pp. 341-350, 2005.

[5] G. Papari, P. Campisi, and N. Petkov, "New families of Fourier eigenfunctions for steerable filtering," *IEEE Trans. on Signal Process.*, vol. 21, no. 6, pp. 2931-2943, 2012.

[6] S. Lucey, R. Navarathna, A. Ashraf, and S. Sridharan, "Fourier Lucas-Kanade algorithm," *IEEE Trans. Pattern Anal. Mach. Intell.*, vol. 35, no. 6, pp. 1383-1396, 2013.

[7] T. Ogawa and M. Haseyama, "Missing texture reconstruction method based on error reduction algorithm using Fourier transform magnitude estimation scheme," *IEEE Trans. on Signal Process.*, vol. 22, no. 3, pp. 1252-1257, 2013.

[8] A. Voropaev, A. Myagotin, L. Helfen, and T. Baumbach, "Direct Fourier inversion reconstruction algorithm for computed laminography," *IEEE Trans. on Signal Process.*, vol. 25, no. 5, pp. 2368-2378, 2016.

[9] W. Hu, G. Cheung, A. Ortega, and O. Au, "Multiresolution graph Fourier transform for compression of piecewise smooth images," *IEEE Trans. on Signal Process.*, vol. 24, no. 1, pp. 419-433, 2015.

[10] X. You, L. Du, Y. Cheung, and Q. Chen, "A blind watermarking scheme using new nontensor product wavelet filter banks," *IEEE Trans. on Image Process.*, vol. 19, no. 12, pp. 3271-3284, 2010.

[11] B. Gaurav, Q. Wu, and B. Raman, "Discrete fractional wavelet transform and its application to multiple encryption," *Inform. Sci.*, vol. 223, pp. 297-316, 2013.

[12] T. Qian and Y. Wang, "Adaptive Fourier series-a variation of greedy algorithm," *Adv. Comput. Math.*, vol. 34, no. 3, pp. 279-293, 2011.

[13] T. Qian, L. Zhang, and X. Li, "Algorithm of adaptive Fourier decomposition," *IEEE Trans. Signal Process.*, vol. 59, no. 12, pp. 5899-5906, 2011.

[14] M. Nahon, "Phase evaluation and segmentation," PhD Thesis, Yale University, 2000.

[15] R. Coifman and S. Steinerberger, "Nonlinear phase unwinding of functions," *J. Fourier Anal. Appl.*, vol. 23, no. 4, pp. 778-809, 2017.

[16] R. Coifman and J. Peyrière, "Phase unwinding, or invariant subspace decompositions of Hardy spaces," *arXiv:1707.04844*, 2017.

[17] T. Qian, "Intrinsic mono-component decomposition of functions: an advance of Fourier theory," *Math. Methods Appl. Sci.*, vol. 33, no. 7, pp. 880-891, 2010.

[18] T. Qian, "Two-dimensional adaptive Fourier decomposition," *Math. Methods Appl. Sci.*, vol. 39, no. 10, pp. 2431-2448, 2016.

[19] T. Qian, Cyclic AFD algorithm for the best rational approximation, *Math. Methods Appl. Sci.*, vol. 37, no. 6, pp. 846-859, 2014.

[20] R. Coifman, S. Steinerberger, and H. Wu, "Carrier frequencies, holomorphy, and unwinding," *SIAM J. Math. Anal.*, vol. 49, no. 6, pp. 4838-4864, 2017.

[21] T. Qian, L. Tan, and Y. Wang, "Adaptive decomposition by weighted inner functions: a generalization of Fourier series," *J. Fourier Anal. Appl.*, vol. 17, no. 2, pp. 175-190, 2011.

[22] W. Mi and T. Qian, "Frequency domain identification: an algorithm based on adaptive rational orthogonal system," *Automatica J. IFAC*, vol. 48, no. 6, pp. 1154-1162, 2012.

[23] W. Mi, T. Qian, and F. Wan, "A fast adaptive model reduction method based on Takenaka-Malmquist systems," *Systems Control Lett.*, vol. 61, no. 1, pp. 223-230, 2012.

[24] D. Alpay, F. Colombo, T. Qian, and I. Sabadini, "Adaptive orthonormal systems for matrix-valued functions," *Proc. Amer. Math. Soc.*, vol. 145, no. 5, pp. 2089-2106, 2017.

[25] D. Alpay, F. Colombo, T. Qian, and I. Sabadini, "Adaptative decomposition: the case of the Drury-Arveson space," *J. Fourier Anal. Appl.*, vol. 23, no. 6, pp. 1426-1444, 2017.

[26] P. Binev, A. Cohen, O. Mula, and J. Nichols, "Greedy algorithms for optimal measurements selection in state estimation using reduce models," *SIAM/ASA J. Uncertain. Quantif.*, vol. 6, no. 3, pp. 1101-1126, 2018.

[27] V. Temlyakov, *Greedy approximation*, Cambridge University Press, 2011.

[28] V. Temlyakov and P. Zheltov, "On performance of greedy algorithms," *J. Approx. Theory*, vol. 163, no. 9, pp. 1134?145, 2011.

[29] S. Mallat and Z. Zhang, "Matching pursuits with time-frequency dictionaries," *IEEE Trans. Signal Process.*, vol. 41, no. 12, pp. 3397-3415, 1993.

[30] R. DeVore and V. Temlyakov, "Some remarks on greedy algorithms," *Adv. Comput. Math.*, vol. 5, no. 2, pp. 173-187, 1996.

[31] A. Dereventsov and V. Temlyakov, "A unified way of analyzing some greedy algorithms," *arXiv:1801.06198*, 2018.

[32] J. Garnett, *Bounded analytic functions*, Academic Press, 1987.

[33] T. Qian, "Boundary derivatives of the phases of inner and outer functions and applications," *Math. Methods Appl. Sci.*, vol. 32, no. 3, pp. 253-263, 2009.

[34] N. Saito and J. Letelier, "Presentation: Amplitude and phase factorization of signals via Blaschke product and its applications," JSIAM, 2009.

[35] W. Mai, P. Dang, L. Zhang, and T. Qian, "Consecutive minimum phase expansion of physically realizable signals with applications," *Math. Methods Appl. Sci.*, vol. 39, no. 1, pp. 62-72, 2016.

[36] T. Qian, H. Li, and M. Stessin, "Comparison of adaptive mono-component decompositions," *Nonlinear Anal. Real World Appl.*, vol. 14, no. 2, pp. 1055-1074, 2013.

[37] L. Tan and T. Qian, "Extracting outer function part from Hardy space function," *Sci. China Math.*, vol. 60, no. 11, pp. 2321-2336, 2017.

[38] S. Marple, "Computing the discrete-time analytic signal via FFT," *IEEE Trans. on Signal Process.*, vol. 47, pp. 2600-2603, 1999.

[39] C. Tan, L. Zhang, and H. Wu, "A novel blaschke unwinding adaptive Fourier decomposition based signal compression algorithm with application on ECG signals," *arXiv:1803.06441*, 2018.

[40] S. Channappayya, "A. Bovik and R. Heath, Rate bounds on SSIM index of quantized images," *IEEE Trans. on Image Process.*, vol. 17, no. 9, pp. 1624-1639, 2008.

[41] C. He, L. Zhang, X. He, and W. Jia, "A new image decomposition and reconstruction approach - adaptive Fourier decomposition," *Int. Conf. on Multimedia Modeling*, 2015, pp. 227-236.

[42] D. Mukherjee, S. Maitra, and S. Acton, "Spatial domain digital watermarking of multimedia objects for buyer authentication," *IEEE Trans. Multimedia*, vol. 6, no. 1, pp. 1-15, 2004.

[43] S. Heidari and M. Naseri, "A novel LSB based quantum watermarking," *Int. J. Theor. Phys.*, vol. 55, no. 10, pp. 1-14, 2016.

[44] R. Zhou, W. Hu, and P. Fan, "Quantum watermarking scheme through Arnold scrambling and LSB steganography," *Quantum Inf. Process.*, vol. 16, no. 9, pp. 1-21, 2017.

[45] A. Jain, U. Uludag, "Hiding biometric data," *IEEE Trans. Pattern Anal. Mach. Intell.*, vol. 25, no. 11, pp. 1494-1498, 2003.

[46] A. Shabir, A. Javaid, A. Nazir, and M. Ghulam, "Robust and blind watermarking technique in DCT domain using inter-block coefficient differencing," *Digit. Signal Process.*, vol. 53, pp. 11-24, 2016.

[47] J. Park, Y. Tai, and I. Kweon, "Identigram/watermark removal using cross-channel correlation," *Proc. IEEE Conf. Comput. Vis. Pattern Recognit.*, 2012, pp. 446-453.

[48] C. Das, S. Panigrahi, V. Sharma, and K. Mahapatra, "A novel blind robust image watermarking in DCT domain using inter-block coefficient correlation," *Int. J. Electron. Commun.*, vol. 53, pp. 244-253, 2014.

[49] S. Lin and C. Chen, "A robust DCT-based watermarking for copyright protection," *IEEE Trans. Consum. Electron*, vol. 46, no. 3, pp. 415-421, 2000.

**Tao Qian** received the PhD degree in harmonic analysis from Peking University, Beijing, China, in 1984. From 1984 to 1986, he worked in Institute of Systems Science, the Chinese Academy of Sciences. Then he respectively worked as Research Fellow and Post-doctoral supervised by Alan McIntosh and Garth Gaudry at Macquarie University and Flinders University of South Australia in Australia until 1992. As a lecturer, he worked at New England University, Australia, from 1992 to 2000. He started working at University of Macau, Macao, China, from 2000 as Associate Professor. He got Full Professorship in 2003, and was Head of Department of Mathematics from 2005 to 2011. From 2013 to 2018 he was appointed as the distinguished professor of the University of Macau. From 2019 he gets Full Professorship in the Macau University of Science and Technology. His research interests include pure analysis, applied and computational harmonic analysis, complex and Clifford analysis, signal analysis, and related areas.



**Yanting Li** received the B.S. and M.S. degrees from Henan University, China. She is currently pursuing the PhD degree with the Faculty of Science and Technology, University of Macau, Macao, China. Her research interests include function approximation theory, signal processing, and image processing.



**Liming Zhang** received the B.S. degree in Computer Software at Nankai University, China and M.S. degree in Signal Processing at Nanjing University of Science and Technology, China. She received her PhD degree in image processing at University of New England, Australia. She is currently an assistant professor in Faculty of Science and Technology, University of Macau. Her research interests include signal processing, Image processing, Computer vision and IT in Education.